Role of the surface intermediates in the stability of basic mixed oxides as catalyst for ethanol condensation

Jorge Quesada, Laura Faba, Eva Díaz, Salvador Ordóñez*

Department of Chemical and Environmental Engineering, University of Oviedo (Faculty of Chemistry), Julián Clavería s/n, 33006 Oviedo, Spain

ARTICLE INFO

Keywords:
Guerbet reaction
DRIFT spectroscopy
Butanol
Aldol condensation
Deactivation

ABSTRACT

The ethanol condensation catalyzed by mixed oxides is studied in this work, considering not only the activity but also the stability of these materials. Concerning to the activity, different weight hourly space velocities (WHSV) were tested, obtaining the highest conversion and 1-butanol selectivity with Mg-Al, mainly at 673 K and a WSHV of 7.9 h^{-1}. On the other hand, dehydration products, observed with Mg-Zr in relevant amounts, limit the results obtained with this material. Deactivation studies were carried out by combining the measurement of reactant and products in the gas phase and in the catalytic surface using spectroscopic techniques (DRIFT). Good stability was observed with both materials at low temperatures (lower than 673 K), whereas at the highest one, Mg-Zr suffers relevant deactivation justified by the permanent adsorption of aldehydes and oxygenated oligomers on the active sites. It has been demonstrated that Mg-Al mixed oxides are promising catalyst for 1-butanol production from ethanol not only in terms of activity, but also in terms of catalyst stability.

1. Introduction

Bioethanol (obtained by fermentation from different biomass feedstocks [1]) is nowadays produced in large amounts, highlighting the United States production (58 millions of cubic meters per year), being around the 60% of the world global production [2]. The large availability, as well as its potential as reactant for different catalytic conversions, justify the high interest for its upgrading as an alternative sustainable raw material, not only for obtaining biofuels [3–5], but also as a platform for the manufacture of other petrochemicals, such as butadiene, butanol or acetone [6]. Among the different technological alternatives [7], the chemo-catalytic route is considered as the most promising one, even above the biological ones [8]. 1-Butanol is the most interesting condensation adduct that can be obtained from bioethanol when its condensation is combined with a partial hydrogenation (Guerbet reaction). It has been proposed as renewable fuel, with better properties than the starting bioethanol (higher energetic density and less hydrophilic behavior) [7]. Besides, 1-butanol can be used as a direct solvent or as starting material for other chemicals production, like acrylic acid, acrylic esters, butyl glycol ether, butyl acetate, dibutylether, etc. [9–12].

First approaches for transforming bioethanol into higher alcohols (butanol, hexanol, etc.) were carried out in liquid phase, using alkali, alkaline-earth hydroxides, transition metal oxides and alkali metal salts as homogeneous catalysts [13,14]. However, alternative heterogeneous processes are currently being studied due to several advantages (e.g., easier separation and recovery of the used catalyst and its possible recycling, lowering corrosion phenomena, reduced environmental constraints) [15,16]. Some authors have proposed three different reaction pathways for this reaction over heterogeneous catalysts: the direct condensation of two alcohol molecules [9,17–19]; the aldehyde (produced by the dehydrogenation of the starting alcohol) and alcohol condensation followed by a hydrogenation step [18,20]; and a four-step reaction process comprising alcohol dehydrogenation to produce aldehyde, subsequent aldol condensation of two aldehyde molecules followed by two hydrogenations [9,21–25]. Analyzing the evolution of the different compounds obtained in previous studies as well as their kinetic ratios, it was concluded that the four-step pathway prevails over the other mechanisms [21–26], and the ethanol condensation is kinetically limited by a previous dehydrogenation step, yielding acetaldehyde [3]. Working in gas phase allows reaching the temperatures needed to overcome this resistance at atmospheric pressure, being the most typical conditions considered in the last studies [25–27].

The considered mechanism for the gas-phase ethanol upgrading, showed in Scheme 1 [5,9,28–30], is a complex process involving different individual steps (dehydrogenations, dehydrations, aldol condensation, hydrogenations, coupling reactions) catalyzed by different active sites. The appropriate tuning of the catalytic properties, would allow shifting the reaction to one or other reaction products. Thus, different catalysts have been used in the ethanol upgrading in order to

* Corresponding author.
E-mail address: sordonez@uniovi.es (S. Ordóñez).

http://dx.doi.org/10.1016/j.apcata.2017.06.001
Received 14 April 2017; Received in revised form 30 May 2017; Accepted 1 June 2017

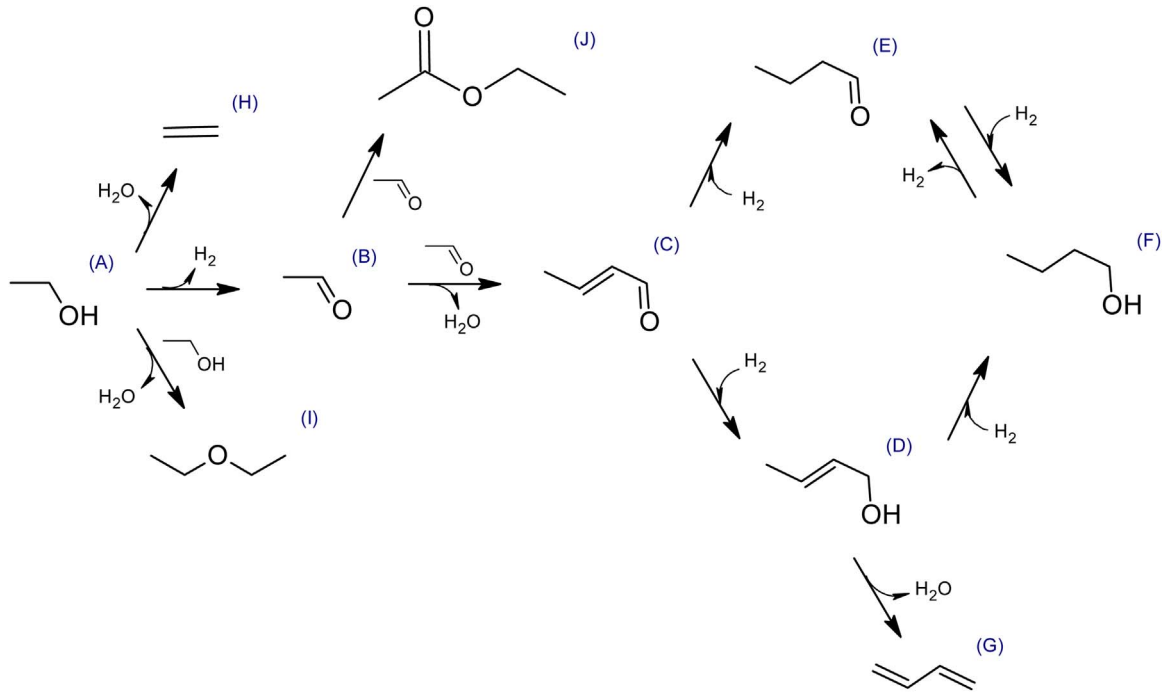

Scheme 1. Proposed reaction mechanism for the ethanol gas-phase condensation [5,9,28–30]. Symbols: (A) ethanol; (B) acetaldehyde; (C) crotonaldehyde; (D) crotyl alcohol; (E) butanal; (F) 1-butanol; (G) 1,3-butadiene; (H) ethylene; (I) diethyl ether; (J) ethyl acetate.

Table 1
Best results reported in the literature for the ethanol gas-phase condensation.

Catalyst	mass or volume	% vol. EtOH	WHSV	T (K)	x (%)	$\phi_{1\text{-butanol}}$ (%)	Reference
MgO	0.3 g	2	*unknown*	673	28	24	[24]
MgO	0.2 g	6.2	1.5 h^{-1}	653	7.9	40	[22]
MgO	0.2 g	8.2	2.5 h^{-1}	673	13	20	[23]
HPA	0.6 mL	20	10,000 L/h	673	22.7	62.4	[27]
HPA	0.06 g	6.2	5 h^{-1}	613	6.6	75	[22]
HPA	0.2 g	20	2 h^{-1}	623	14	71	[5]
HPA	0.3 g	5.6	0.7 h^{-1}	603	17.1	63.2	[18]
Mg_yAlO_x	0.2 g	9	1 h^{-1}	573	9.7	42.6	[30]
Mg_yAlO_x	*unknown*	9	0.4 h^{-1}	573	19	53	[9]

obtain a specific product, such as zeolites [17,31], metal oxides [20,26,32], metal mixed oxides [9,28], transition metal in the presence of basic compounds [10,33,34], and hydroxyapatites (HAP) [5,19,23]. Although results obtained with these materials cannot be directly compared (different conditions were tested in each work), best results previously reported in the literature are summarized in Table 1. As it can be observed, the HPAs highlight because of their high 1-butanol selectivity, although conversions lower than 25% were obtained in any case. On the other hand, best results obtained with Mg-Al mixed oxides are not so different, with a slight decrease in the 1-butanol selectivity but similar conversions in spite of working at softer reaction conditions and with a higher ethanol concentration in the feed stream. Despite the promising results of some of these materials (mainly mixed oxides and HAPs), there are not systematic studies about the stability of heterogeneous materials in this reaction. The only study that is reported in the literature that considers the evolution of the activity with the time on stream does not provide mechanistic justifications enough to extrapolate these results to a general behavior of these catalysts [5].

Considering the relevance of the catalyst stability, a deep deactivation study is needed for evaluating the feasibility of these technologies. In order to analyze the dynamics of the catalytic surface (changes in the morphology and physico-chemical properties), the information provided by different techniques must be gathered (physisorption, temperature-programmed oxidation, X-ray diffraction, etc.). Besides, diffuse reflectance infrared fourier transform (DRIFT) spectroscopy provides relevant information about the interaction of reactants, products and intermediates with the catalyst surface [35–38]. This technique allows analyzing the evolution chemical moieties adsorbed on the catalytic surface, being possible to identify the intermediates or final products present in these interactions.

The main aim of this work is to analyze the catalytic stability in the gas-phase ethanol condensation. Mixed oxides proposed as catalysts for this study were chosen considering the previous knowledge about these materials in our research group [28], and the possibility to modify the ratio between both cations to enhance the catalytic results. In addition, Mg-Al was previously proposed as catalyst for this reaction [9,24], but its deactivation has been scarcely studied. In addition, although the higher acidity of Mg-Zr (compared to Mg-Al with similar proportions) suggests a worse performance [39], the stability of this material has been previously studied in other gas-phase condensations with promising results [38]. Results obtained are related to the different surface properties of these materials, identifying the active sites controlling the reaction. The stability and deactivation causes were then analyzed considering the optimum conditions previously determined for both materials. Using different characterization techniques as well as the DRIFT spectroscopy, and comparing the data with the reaction results, the evolution of different compounds in the surface is analyzed and correlated to the activity loses, comparing the behavior of two materials with different surface chemistry.

2. Materials and methods

2.1. Catalysts preparation

Mg-Al mixed oxide (Mg/Al = 3) were obtained by the calcination of the corresponding hydrotalcites. The hydrotalcites were synthesized by co-precipitation of the Mg and Al nitrates at low supersaturation under sonication, following the procedure previously optimized by León et al. [28]. The gel was precipitated by increasing the pH to 10 and it was aged at 353 K for 24 h. The solid phase was then isolated by centrifugation, washed with deionized water to pH 7 and dried at 383 K for

24 h. The mixed oxide was obtained by the thermal treatment under air flow of the corresponding hydrotalcites from 293 to 973 K with a rate of 5 K min^{-1}, holding this temperature for 5 h.

Mg-Zr mixed oxide (Mg/Zr = 4) was prepared from nitrate precursors using the sol-gel method detailed in our previous work [40]. The gel was aged at 353 K during 24 h, filtered, washed to pH 7 and dried at 383 K for 24 h. Finally, the mixed oxide was obtained by thermal treatment in helium flow, following a temperature program from 293 to 873 K with a rate of 5 K min^{-1} and holding the final temperature during 3 h.

2.2. Fresh catalysts characterization

Morphologic parameters were analyzed by N_2 physisorption at 77 K in a Micromeritics ASAP 2020 by using the Brunauer-Emmett-Teller (BET) method to calculate the surface area, and the Barret-Joyner-Halenda (BJH) method to determine pore volume and diameter.

Basicity and acidity were determined by temperature programmed desorption (TPD) technique, using a Micromeritics 2900 TPD/TPR. In both cases, 20 mg of sample were pre-treated in He flow and saturated with CO_2 or NH_3 to measure the basicity or acidity, respectively. The evolution of CO_2 and NH_3 signals were monitored in a Pfeiffer Vacuum Omnistar Prisma mass spectrometer while the temperature was increased at 2.5 K min^{-1} from 298 to 973 or 873 K, for Mg-Al or Mg-Zr, respectively.

The crystallographic structure of the mixed oxides was determined by X-ray diffraction (XRD) using a Philips PW 1710 diffractometer, working with a CuK_α line (1.54 Å) in the 2θ range between 5 and 80°, at a scanning rate of 2° min^{-1}.

The surface composition of the samples was determined by X-ray photoelectron spectroscopy (XPS), using a SPECS system equipped with a Hemispherical Phoibos detector operating in a constant pass of energy, with MgK_α radiation ($h\nu$ = 1253.6 eV). The samples were fixed to the sample holder with a carbon adhesive tape. The background pressure in the analysis chamber was kept below $4{\cdot}10^{-9}$ mbar during data acquisition. As samples are non-conducting, surface neutralization during measurements was required.

2.3. Catalytic activity studies

Ethanol conversion experiments were performed between 473 and 723 K (with an interval of 50 K) in a 0.4 cm i.d. U-shaped fixed bed quartz reactor placed in a controlled electric furnace. The catalyst (100–250 mg as function of the reaction; 250–355 μm) was placed over a plug of quartz wool and a thermocouple was placed inside the catalyst bed. Solid was pre-treated at 773 K for 1 h in helium flow before each reaction. Absolute ethanol was injected by a syringe-pump in the helium flow, inducing the vaporization in situ, obtaining a 32 vol.% of ethanol, fed to the reactor at 0.02 L min^{-1} (STP), with values of weight hourly space velocity (WHSV) from 4.7 to 11.8 h^{-1}. Outgoing gases were on-line analyzed by gas chromatography using a HP6890 Plus, equipped with a flame ionization detector (FID). A TRB-5MS capillary column (30 m, 0.25 mm) was used as stationary phase. The identification of each compound was carried out using commercial standards and corroborated by GC–MS (Shimadzu QP-2010) using the same column and methodology as in the GC-FID.

Conversions (x) were calculated from the ethanol concentration at the reactor inlet and outlet. Selectivities (φ) were calculated as the ratio between the concentration of each compound and the sum of the concentration of all the reaction products (considering the carbon atoms of each compound). In order to better analyze the activity, yields (η) for different products were also considered, according to the following equation:

$$\eta_i = x{\cdot}\varphi_i$$

Carbon balances were checked by comparing the total amount of carbon atoms at the reactor inlet and outlet, considering only the identified products.

DRIFT spectroscopy was carried out using a Thermo Nicolet Nexus FT-IR equipped with a Smart Collector Accessory and a MCT/A detector, configured to record with a resolution of 4 cm^{-1} and to collect 60 scan/spectrum. The catalyst sample (20 mg) was placed inside the catalytic chamber where the temperature was controlled by a thermocouple. Samples were pre-treated at 773 K for 1 h in helium flow. Spectra were recorded in the 4000–650 cm^{-1} wavenumber range, after subtraction of the KBr standard background. All the signals were converted into Kubelka-Munk units to obtain semi-quantitative results. Spectra were collected at the same temperatures as in the reactor in order to compare the evolution of both gas and solid phase. The identification of each band was obtained by stepwise TPD-DRIFT spectroscopy. In these experiments, spectra were collected in He flow after a previous saturation step (30 min) using the probe molecules and a bubbler.

2.4. Catalytic stability studies

Catalyst stability was studied at temperatures of 673 and 723 K in the same experimental setup described above for the reaction studies. Conversion, selectivities and carbon balances evolution were followed as a function of time on stream analyzing the gas-phase for 8 h by gas chromatography. DRIFT spectroscopy measurements were recorded at 673 and 723 K each 10 min during 8 h for both Mg-Al and Mg-Zr catalysts.

Solids obtained after 8 h on stream at 723 K were homogenized and analyzed in a TG-SC instrument (Setaram, Sensys) using α-alumina as inert reference material. Samples (20 mg) were treated in a nitrogen flow (20 mL min^{-1}) with a temperature program of 5 K min^{-1} from 298 to 923 K. Changes in the crystallographic structure and surface area of these catalysts were studied by analyzing the spent samples using the same equipment and conditions than for the fresh catalysts. Additionally, 150 mg of the spent materials were added to 2 mL of tetrahydrofuran and the liquid phases were analyzed by GC–MS after sonication for 30 min at room temperature.

3. Results and discussion

3.1. Optimization of reaction conditions

First studies were carried out to identify the best reaction conditions, analyzing the behavior of Mg-Al at different temperatures and different WHSV. The effect of the WHSV on catalyst performance (ethanol conversion and 1-butanol yield) is depicted in Fig. 1. The external mass transfer coefficient and the internal diffusivity – evaluated from Thiele modulus (Φ) – were calculated in order to discard the presence of diffusional effects. Results obtained were compared with the limit values considered by Davis and Davis [41]. Taking into account that same particle size was used in all the studies (250–355 μm), the reaction temperature is the only operation parameter to be considered (the influence of the WHSV is negligible). Studies were carried out considering the maximum conversion observed (53%, most adverse case) obtaining values of external mass transfer effect almost seven orders of magnitude lower than the limit to consider this effect as relevant. Regarding to the Thiele modulus, it is lower than 0.02 for all the performed experiments. As a consequence, mass transference limitations were discarded and results can be directly related to the activity of this material.

As expected, ethanol conversion increases at increasing temperatures, being more evident the influence of the catalytic mass at temperatures over 623 K, reaching maximums over 52% at 723 K. At these conditions, the obtained carbon balances were in all the cases above 70% (82.6, 73.2, 80.1 and 75.1% for 11.8, 7.9, 5.9 and 4.7 h^{-1}, respectively). The GC–MS analyses corroborate that these values are due

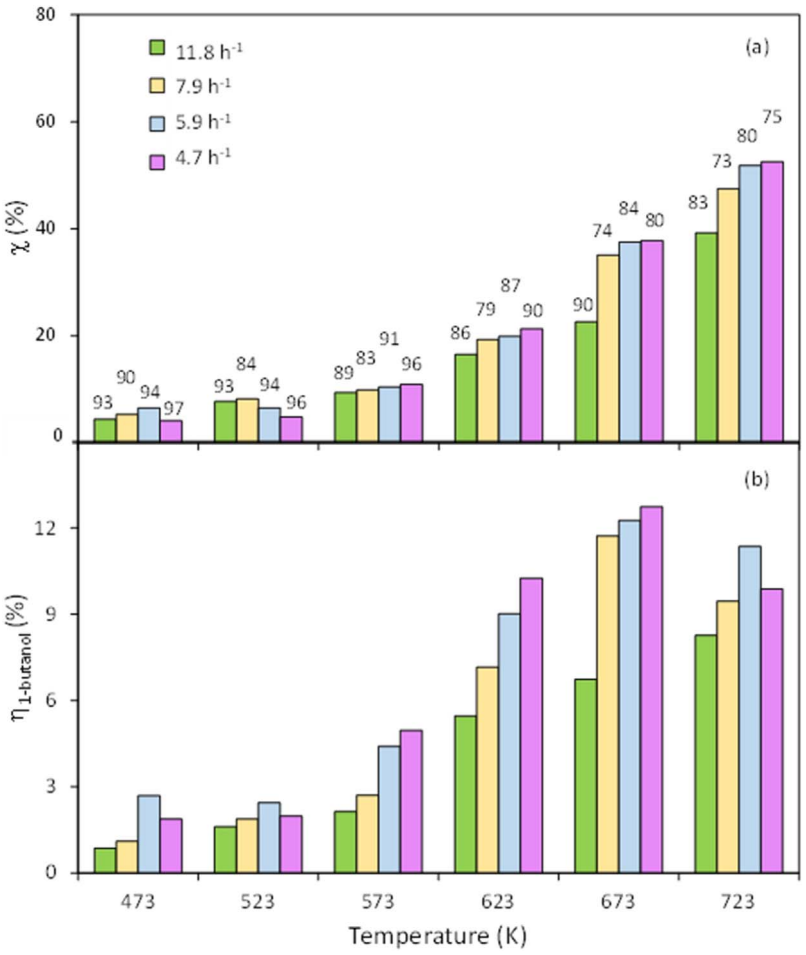

Fig. 1. Comparison of ethanol conversion (a) and 1-butanol yields (b) obtained as function of the temperature in the gas phase ethanol condensation catalyzed by Mg-Al using different WHSV of 11.8, 7.9, 5.9, and 4.7 h^{-1}. (catalyst mass: 100, 150, 200, and 250 mg; 32 vol.% of ethanol). Numbers over the conversion bars indicate the carbon balance closure in terms of percentage.

to the presence of different unsaturated alcohols, olefins and aromatics obtained as side products of the main mechanism. In order to identify the best operation conditions, butanol yields must be also considered. Values obtained in the range 623–723 K were the highest in all the cases, reaching the maximum values at 673 K (6.7, 11.7, 12.3 and 12.7% with 11.8, 7.9, 5.9 and 4.7 h^{-1}, respectively) except for the WHSV of 11.8 h^{-1} which was higher at 723 K (8.3 %). Regardless the space velocity, the yield decreases after this maximum, indicating that main reaction is not favored at the highest temperatures. According to the butanol yields, a WHSV of 7.9 h^{-1} was considered as the optimum one (the slight increase obtained at lower WHSV values is not compensated by the high increase in the catalytic mass needed).

In order to gain further understanding on the reaction mechanism, Fig. 2 shows the gas-phase analyses for the reaction catalyzed by 150 mg (WSHV = 7.9 h^{-1}), in terms of ethanol conversion, carbon balance and evolution of the selectivity for the different compounds involved in the reaction. Similar trends were obtained at the other WHSV considered, being the profiles included as Supplementary material (Fig. S1). Selectivities evolution is congruent with the considered mechanism (Scheme 1). Thus, acetaldehyde (first intermediate) is the main product (66%) at the lowest temperature, decreasing as temperature increases, reaching values lower than 32% at 723 K. The relevance of the two primary side reactions (formation of ethylene and diethyl ether from ethanol) increases at the highest considered temperatures. However, the selectivity of diethyl-ether never reaches values higher than 2%, whereas more than 35% of ethylene was obtained at the same conditions. Concerning to the main condensed intermediates (labelled as C-butenal-, E-butanal- and D-crotyl alcohol- in Scheme 1), they were detected with very low selectivities in all the cases, being only relevant the selectivities of two final products: 1-butanol (the desired one) and 1,3-butadiene. At all the reaction conditions tested, 1-butanol selectivities were always higher than 20%, reaching a maximum at 623 K, with a 37.1% selectivity. Selectivity decreases at highest temperature because of the presence of side reactions. In fact, the amount of 1-butanol obtained increases at increasing temperatures, but the product distribution is less selective at these conditions. Finally, the selectivity of 1,3-butadiene increases mainly at the highest temperatures, with a final value of 5.7% at 723 K. The decrease in the carbon balance closure as the temperature increases (from 90% at 473 K to 63.5% at 723 K) can be explained by the formation of different undesired products. At high temperatures, the Guerbet reaction can produce higher alcohols mainly with an even number of carbon because of subsequent aldol condensations (selectivities to 2-ethylbutanol, 1-hexanol, 2-ethylhexanol, and 1-octanol are summarized in Table S1), and also the role of dehydration reactions is more relevant, yielding water [42]. In the same way, C—C bond cleavage reactions are more likely to take place at the highest temperatures [42,43], justifying the presence of molecules with an odd number of carbon atoms. In good agreement with these lateral reactions, propanone, pentanol, hexenol and other alcohols or aldehydes and aromatic compounds were detected by GC–MS.

The distribution of quantifiable minor reaction products is detailed in Fig. 3. In global terms, two maxima are detected (at 523 and 723 K), but corresponding to very different situations. Despite the reaction conditions, crotonaldehyde is not observed at quantifiable amounts, indicating that the first hydrogenation of this compound is fast. However, the resulting crotonaldehyde hydrogenation product (crotyl alcohol or butanal) is strongly conditioned by the reaction temperature. At low temperatures, prevails the crotyl alcohol (selectivities close to 10%), whereas almost 5% of butanal is obtained at 723 K. Considering

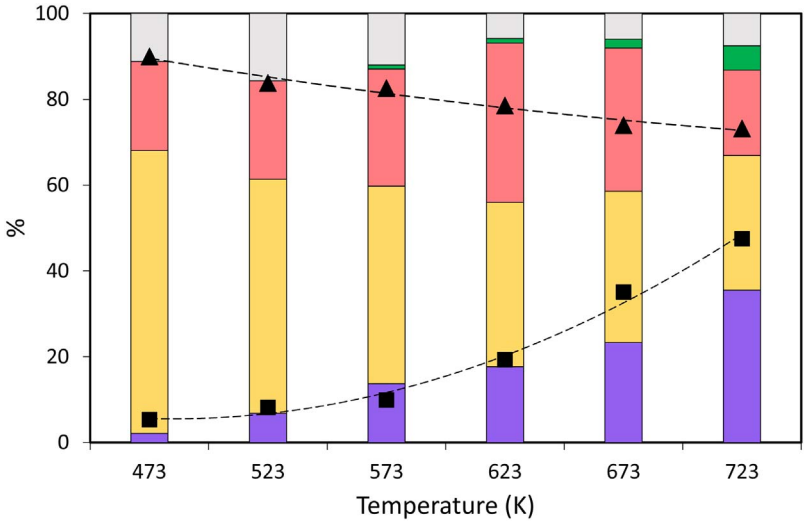

Fig. 2. Results of the gas phase ethanol condensation catalyzed by Mg-Al at different temperatures. (WHSV = 7.9 h^{-1}; catalyst mass: 150 mg; 32 vol.% of ethanol). Symbols correspond to ethanol conversion (■) and carbon balance (▲). Bars correspond to selectivities of ethylene (purple); acetaldehyde (yellow); 1-butanol (pink); 1,3-butadiene (green) and others (grey). *"Others" includes minor reaction products (crotonaldehyde, crotyl alcohol, butanal, diethyl ether and ethyl acetate).* (For interpretation of the references to colour in this figure legend, the reader is referred to the web version of this article.)

that both steps are hydrogenation reactions, two different mechanisms are suggested. The first one (from crotonaldehyde to crotyl alcohol) is promoted by the Meerwein-Ponndorf-Verley (MPV) reduction. On the other hand, the second route (to obtain the butanal) implies the hydrogenation of one C=C double bond. Considering that no molecular hydrogen is fed, this step requires the hydrogen released in the ethanol dehydrogenation. Experimental results suggest that the higher polarity of the interaction between the aldehyde and the catalytic surface enhances the role of the MPV mechanism, mainly at the lowest temperatures. This analysis is not so evident at higher temperatures in which the relevance of the equilibrium between butanal and 1-butanol (hydrogenation-dehydrogenation) is more relevant.

Results obtained with the Mg-Al at the best considered conditions (WHSV = 7.9 h^{-1}) were compared with the activity of Mg-Zr, a mixed oxide with a tested activity in aldol condensation [40]. Fig. 4 shows the evolution of conversion and selectivities of main products as function of the temperature. In general terms, conversion values are quite similar than those obtained with Mg-Al at same conditions. Moreover, it was observed a lower influence of the temperature with the Mg-Zr, except at the highest ones (623–723 K) at which conversions began to increase to a larger extent causing that the conversion increase was not as gradual as with the Mg-Al (increases of 140 and 194% between 623 and 723 K with Mg-Al and Mg-Zr, respectively). Conversion values were used to compare the activation energies as well as the pre-exponential factors obtained with both materials, considering that the disappearance of ethanol follows an apparent first order kinetics. There is a good fitting between experimental data and this model, as it is demonstrated in Fig. S2, in the Supplementary material. The activation energy values obtained were 38.8 and 44.1 kJ mol^{-1}, for Mg-Al and Mg-Zr respectively, whereas the pre-exponential factors were $1.60{\cdot}10^{-3}$ and $2.76{\cdot}10^{-3}$ $m^3\ s^{-1}\ kg\ cat^{-1}$, respectively, justifying the higher activity of Mg-Al by its lower activation energy. These values are congruent with data previously reported for this type of reactions, as for example 37 kJ mol^{-1} for the acetaldehyde aldol condensation catalyzed by TiO_2 [44], or 42 kJ mol^{-1} for the reaction of ethanol to 1,3-butadiene catalyzed by metal-promoted magnesia silicate catalyst [45].

Carbon balances obtained with Mg-Zr were in all the cases higher than 64%, with a decreasing profile congruent with the presence of lateral reactions at the highest temperatures. Taking into account that this decrease is more marked with Mg-Zr, it suggests a higher relevance of these side condensations (selectivities to higher alcohols summarized in Table S2), obtaining a plethora of alcohols and aldehydes in the GC–MS analysis. Concerning to the 1-butanol yield, similar trend was also observed, but the maximum selectivity (at intermediate temperatures) was considerably lower (2.4% at 673 K). At high temperatures, the amount of ethylene (undesired product) was significantly higher with Mg-Zr (60% at 723 K). This compound was not observed at lower temperatures, in good agreement with the behavior previously observed by Di Cosimo and coworkers [9], with other Mg-Al mixed oxides. In the same way, the amount of diethyl-ether (other side product that was no significantly observed with Mg-Al) reached selectivities higher than 11.5% when Mg-Zr was used as catalysts (at 723 K). Finally, the

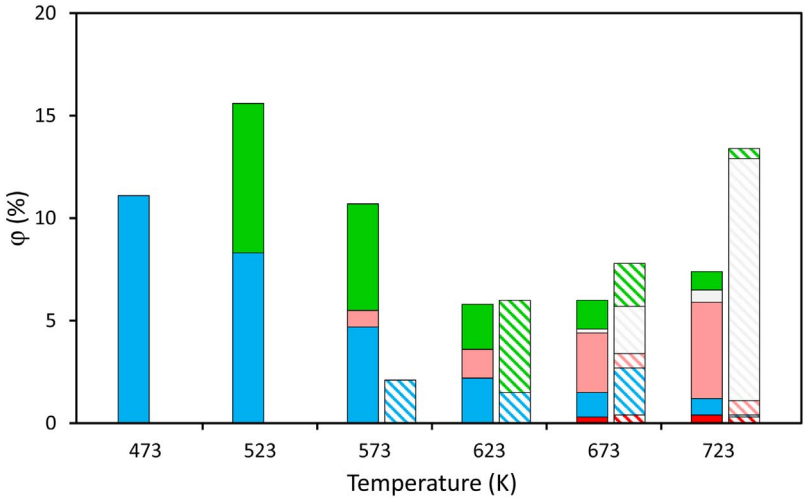

Fig. 3. Distribution of minority compounds obtained in the gas phase ethanol condensation catalyzed by Mg-Al (filled bars) and Mg-Zr (striped bars) as function of the temperature. (WHSV = 7.9 h^{-1}; catalyst mass: 150 mg; 32 vol.% of ethanol). Symbols: crotonaldehyde (red); crotyl alcohol (blue); butanal (pink); diethyl ether (grey); ethyl acetate (green). (For interpretation of the references to colour in this figure legend, the reader is referred to the web version of this article.)

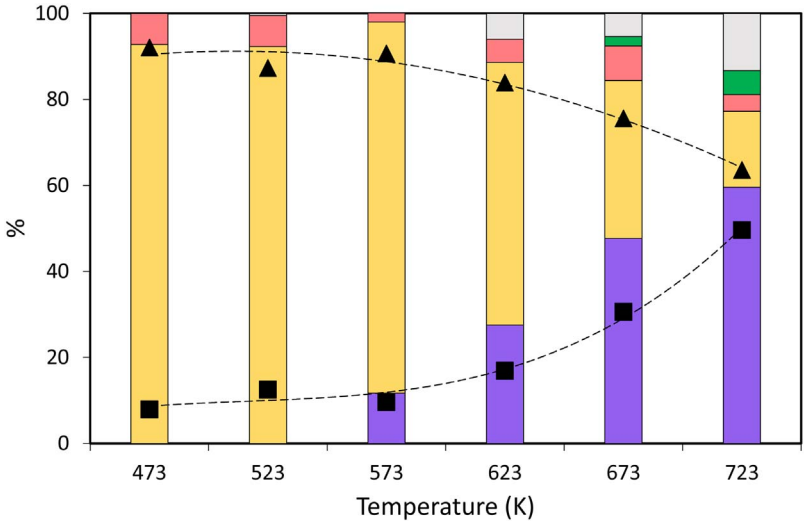

Fig. 4. Results of the gas phase ethanol condensation catalyzed by Mg-Zr at different temperatures. (WHSV = 7.9 h^{-1}; catalyst mass: 150 mg; 32 vol.% of ethanol). *(See Fig. 2 for codes).*

selectivity of 1,3-butadiene was very similar in both cases, and only significant at the highest temperatures (5.6%). Minority compounds are also detailed in Fig. 3. Comparing these results with those obtained with Mg-Al, higher temperatures are needed to detect these products when Mg-Zr is used, highlighting the diethyl ether as the main one (11.8% at 723 K). Concerning to the other compounds considered, similar trends were obtained but at higher temperatures and with lower selectivities.

3.2. Surface chemistry

In order to gain further understanding on the catalysts behavior in the reaction, the evolution of the different species adsorbed on the catalytic surface was followed using DRIFT spectroscopy. Fig. 5 shows the spectra recorded at the same reaction conditions when Mg-Al (Fig. 5a) or Mg-Zr (Fig. 5b) were used as catalyst in order to determine the different adsorption modes of ethanol and their reaction products. For this reaction, authors assign the adsorption bands by analogy with other works [20,25,27,32,45]. However, although some of them contrasted their data with similar materials (Davis and coworkers, MgO with regard to MgO) [32], others used results obtained with different catalysts (Mella and coworkers, MgO with regard to Al_2O_3) [20]. This last mode of band assignation is not entirely appropriate, since the surface chemistry of different materials is also different and, consequently, the characteristic adsorption bands of the molecules adsorbed over them too. Furthermore, attributing the vibration mode of the adsorption bands comparing with the gas phase data always needs an adjustment because chemisorbed and even physisorbed species change the position of the adsorption band in the spectra. Nevertheless, the differences in the wavenumbers of the same characteristic bands when using different materials are comparable as those observed regarding to the gas phase (Rekoske and Barteau, TiO_2 with regard to SiO_2 and gas phase data) [46]. Therefore, in this work the vibration mode of each adsorption band, shown by stepwise TPD-DRIFT spectroscopy experiments, has been assigned (and summarized in Table S3) comparing them with the results proposed for each molecule in the gas phase by Shimanouchi [47], since there are not previous infrared works with these molecules using Mg-Al or Mg-Zr mixed oxides as catalyst. In general terms, and with both materials, the intensities of most of the bands decrease with the temperature. This fact is congruent with the exothermicity of the adsorption process. Besides, this decrease is usually also associated with a slight displacement of the maximum, suggesting that more than one molecule with same functional groups are adsorbed on the catalytic surface with the same vibration mode.

As it could be expected, main bands are associated to the formation of surface alkoxides (presumably ethanol but with some signals in common with other products, see Table S3), highlighting the signals observed at 1050 cm^{-1} and at 940 cm^{-1}. The first one is identified as the CO stretching mode and it is the main one at low temperatures for both materials. This signal decreases sharply as the temperature increases, mainly in the case of Mg-Al, being almost negligible at 723 K. In the case of Mg-Zr, this decrease is softer, being the intensity still relevant at temperatures above 673 K. This different behavior is congruent with the results in gas phase and the highest ethanol conversion observed with the Mg-Al. The signal at 1050 cm^{-1} is also relevant in the adsorption of other chemicals, such as crotyl alcohol, butanol and diethyl ether. In any case, the total disappearance at the temperatures in which the selectivity of these compounds is higher suggests that these compounds are not permanently adsorbed on the catalytic surface by this functional group. The second band related to the ethanol is centered on 940 cm^{-1}, related to CH_3 rocking and C—H bending vibration modes present in different molecules involved in this reaction. The decrease of this band at increasing temperatures is also evident, mainly with the Mg-Al, but this decrease is lower than in the peak at 1050 cm^{-1}. There is a complex area band around 1300–1800 cm^{-1} in which adsorption of different species are overlapped. The band at 1380 cm^{-1} is identified as the C—H bending mode of aldehydes. The high intensity of this band at low temperatures in the Mg-Al is congruent with the highest activity of this material, being associated to the presence of aldehyde (first intermediate of the main reaction). The area of this peak decreases at medium temperatures (congruent with the advance of the reaction) and the maximum slightly moves to higher wavenumbers, indicating the adsorption of other carbonyls with higher molecular weight (crotonaldehyde and butanal). These results suggest that at low temperatures the adsorption prevails over the desorption and the final products are not detected in the gas phase despite that ethanol conversion observed. Signals around 1580–1590 cm^{-1} are related to the formation of compounds with C=C bonds obtaining by aldol condensation of acetaldehyde and crotonaldehyde [45]. The highest intensity observed in the spectra of Mg-Zr, mainly at high temperatures, is in good agreement with the gas-phase results, with more selectivity to higher alcohols (Tables S1 and S2) produced from these aldol condensation products. Two minor-role bands at 1660 and 1740 cm^{-1} appear only at the highest temperatures. These wavenumbers are identified to the C=C and C=O stretching modes of crotonaldehyde and crotyl alcohol, and crotonaldehyde and butanal, respectively. These signals are in good agreement with the previous one at 1380 cm^{-1}, being the two main adsorption modes of aldehydes compounds. The highest intensity observed with Mg-Zr suggests a permanent adsorption of these compounds (their yields in gas phase

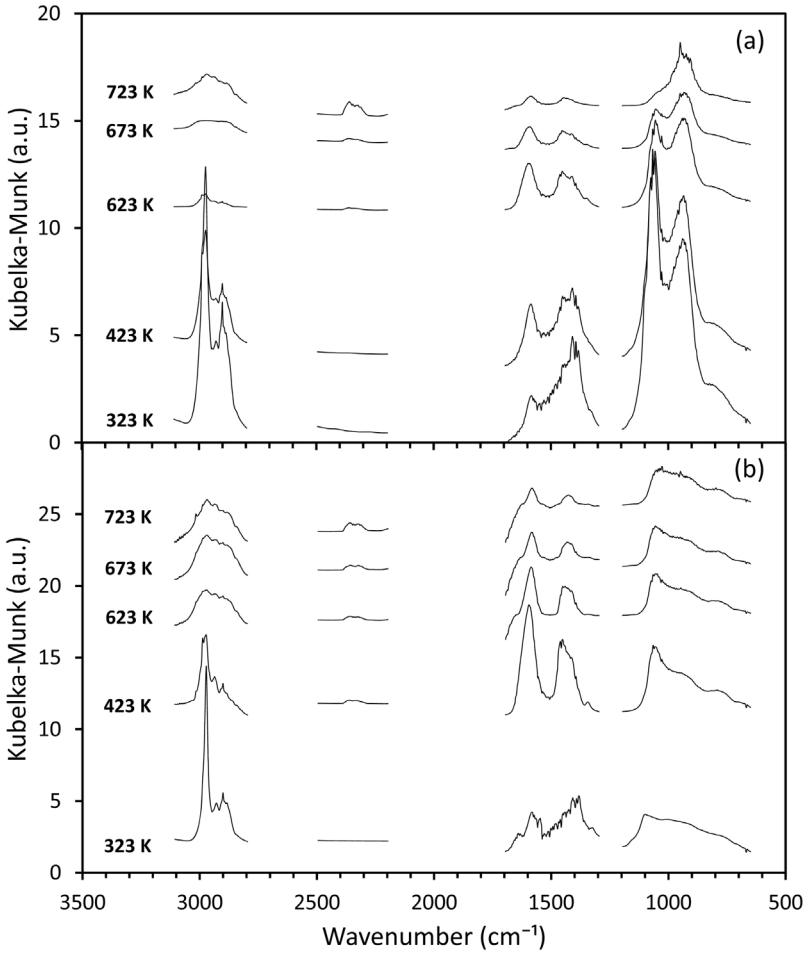

Fig. 5. Evolution with the temperature of the characteristic bands of adsorbed compounds in the ethanol gas phase condensation when (a) Mg-Al or (b) Mg-Zr is used as catalyst.

was always lower than 3%), making more difficult their reaction to obtain the 1-butanol.

The presence of side-reaction that produce C_3, C_5, and other odd carbon number unsaturated alcohols and olefins (detected by GC–MS) was also observed by DRIFT spectroscopy, being related to the signals at 2380 cm^{-1} and in the range of 2800–3100 cm^{-1}. The first one is associated to the CO_2 [47]. The presence of this molecule in this reaction has been previously demonstrated by Dömök and coworkers [42]. According to their mechanism, aldehydes can be transformed into the corresponding carboxylates if water is present in the reaction atmosphere. This carboxylate is unstable, obtaining the CO_2 by its decomposition. In this case, water is obtained in the dehydration reactions and acetaldehyde is the first intermediate in the main mechanism. On the other hand, the wide range 2800–3100 cm^{-1} is related to the CH_3 and CH_2 stretching modes, being their intensity proportional to their carbon chain length. The intensity of all these bands is considerably higher in the Mg-Zr spectra, suggesting a higher relevance of these side reactions. In good agreement with this hypothesis, there is a continue increase in the band at 3680 cm^{-1}, identified not only as the OH stretching mode related to the presence of long-chain alcohols, but also as a vibration mode of water [47]. Besides, there is a band around 730 cm^{-1}, associated with the CH_2 rocking mode produced in molecules with four or more CH_2 groups [48], that only appears in the Mg-Zr.

The differences between both materials, in both gas and solid phase, can be explained considering the morphological and physico-chemical properties of their catalytic surfaces. Main results obtained with the different characterization techniques are summarized in Table 2. Concerning to the physisorption results, the surface area obtained with Mg-Al was more than three times higher than the area obtained with the Mg-Zr, being both catalysts mesoporous solids. Similar values of pore volume were obtained, whereas Mg-Zr has higher pore diameter than Mg-Al. In any case, reported values discard the presence of diffusional limitation. The highest crystallinity was observed in the XRD spectra of Mg-Zr (Fig. 6), observing more intense and narrower peaks than in the Mg-Al, being congruent with values obtained in the surface area. In both cases, periclase is the main crystalline phase (JCPDS 45-946; 2θ = 43, 63 and 78°), indicating that a different crystallinity is not the key factor in this reaction. Furthermore, small peaks related to tetragonal zirconia (JCPDS 42-1164; 2θ = 30, 51, 59, and 74°) were also distinguished in Mg-Zr. Peaks associated to alumina are not observed in the Mg-Al, suggesting that most of this metal is presented as Mg-substituent in the internal structure of the periclase. This hypothesis is congruent with the higher width of these peaks in Mg-Al, because of the distortion produced by the Al^{3+}. In this catalyst there is also a small peak centered at 2θ = 36° that can correspond with the spinel structure (JCPDS 21-1152; 2θ = 36.9°), typical structure of Mg-Al mixed oxide. In good agreement with XRD results, XPS analyses reveal a surface content of Al about 35% for Mg-Al, whereas the surface amount of Zr is much lower. XPS results also indicate higher proportion in surface basis of oxygen in the Mg-Zr (almost 60% whereas there is only 38% with the Mg-Al). This higher proportion of oxygen, increase the difficult to obtain acid-basic pairs on this surface. As it was previously mentioned, this coordination between acid and basic sites is needed to stabilize key steps in the reaction. As a consequence, the activity of this material is lower and side reactions promoted by basic sites (isolated ones), such as dehydrations via unimolecular elimination conjugate base (E_{1CB}) [9], are enhanced. This fact justifies the higher amount of ethylene and diethyl ether obtained in the reaction catalyzed by Mg-Zr. Besides the high volatility of these compounds, these products cannot be easily observed by DRIFT because their main bands (according to the

Table 2
Main results of the fresh catalysts characterization: morphological properties, density and distribution of the acid and basic sites, XPS O^{1s} binding energy, and XPS surface composition.

Catalyst	Morphological properties			Acid sites (μmol g^{-1}), [T (K)]			Basic sites (μmol g^{-1}), [T (K)]			XPS O^{1s} B.E. (eV)	XPS surface composition (%)			
	S (m^2 g^{-1})	D_p (Å)	V_p (cm^3 g^{-1})	weak	medium	strong	weak	medium	strong		Mg	Al	Zr	O
Mg-Al	226	135	0.74	11.3 [345,370]	12.5 [450]	41.8 [630,800]	49.7 [340]	71.7 [400]	238.6 [630,670,800]	528.8	26.9	34.7	–	38.4
Mg-Zr	77	305	0.80	52.0 [360]	41.3 [440]	47.2 [630,750]	34.7 [380]	68.7 [450]	52.5 [627]	529.1	41.0	–	0.4	58.6

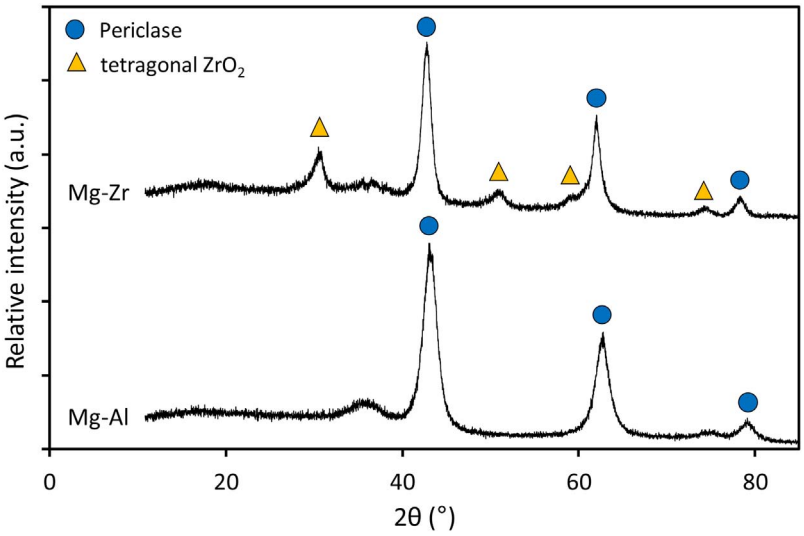

Fig. 6. XRD diffractograms of Mg-Zr, and Mg-Al.

literature the strongest ones are located at 1444, 2989 and 3106 cm^{-1}) [47] overlap with other signals related to other main products.

The concentration and strength-distribution of basic and acid sites analyzed by TPD of CO_2 and NH_3, respectively (Table 2) contributes to justify the different activities in the main route observed with both materials. The 1-butanol formation implies a first dehydrogenation of ethanol, the aldol condensation of the resulting acetaldehyde and two further steps of hydrogenation. According to the literature [9], these three reactions are catalyzed by different active sites and there is not good agreement about the key parameter of the whole process.

The dehydrogenation of ethanol requires a good balance between medium strength acid and basic pairs in order to activate the C—H bond (acid site), thus it is adsorbed as an ethoxide and then dehydrogenated (basic site). Since both materials show similar medium basicity, being more relevant the differences in the medium acidity, it can be inferred than a minimum basicity/acidity ratio is needed to favor the equilibrium between the proton and the ethoxide adsorbed. Besides, as it was suggested by XPS results, not all the basic sites of Mg-Zr take part of acid-basic pairs. Same good distribution is also required in the aldol condensation of two acetaldehyde molecules to obtain the crotonaldehyde [49,50]. Considering that no significant amounts of this compound are detected in any case, it can be concluded that this compound is quickly transformed into the following intermediates of the main reaction.

Acid-basic pairs with a strong basic character are needed for the last hydrogenation steps of the Guerbet reaction [28], justifying that the 1-butanol yield is much higher with Mg-Al. This type of active sites has been also reported as responsible of side-reaction to obtain alcohols with longer chains via crotonaldehyde aldolization [51]. Despite this competitive effect, the relevance of the oligomerizations is not so high, indicating that the hydrogenation of crotonaldehyde is easier than its condensation (selectivities to higher alcohols much lower than selectivity to 1-butanol).

Concerning to the specific role of the acidity, main differences are related to the weak and medium sites. Desorption temperatures are very similar in both cases, indicating a similar strength, but the concentration of these sites is almost four times higher for Mg-Zr. These sites mainly promote the dehydration of alcohols to olefins via E_2 mechanism [9]. According to the Scheme 1, two different dehydrations to olefins occur in the gas-phase ethanol self-condensation, the ethanol dehydration to ethylene and the crotyl alcohol dehydration to 1,3-butadiene. As a consequence, the large amount of ethylene obtained with Mg-Zr is the consequence of the coexistence of both dehydration mechanism E_{1CB} and E_2, mainly at the highest temperatures. Besides, this fact is also responsible of the relative high 1,3-butadiene yield obtained with this material at medium-high temperatures. This role is no so evident, mainly at high temperatures, because it is conditioned by the previous steps; but there is a clear competition with the crotyl alcohol hydrogenation at lower temperatures, preventing the 1,3-butadiene appearance. In good agreement, the ratio 1-butanol/1,3-butadiene is four times lower with the Mg-Zr than with the Mg-Al (15.9 and 3.6 at 623 K, for Mg-Al and Mg-Zr, respectively), in same ratio than the acidity differences.

Diethyl ether formation is also produced by dehydration of two ethanol molecules which are firstly coupled, taking place on the same active sites as alcohol hydrogenation and aldol condensation [9,40,50]. This competition between different reactions implies that ethylene yield was much higher than diethyl ether for any temperature even though dehydration to olefins has a higher activation energy than dehydration to ethers [9]. The more acidic character (which promote the dehydration process) of the Mg-Zr catalyst entails that diethyl ether was only significantly observed at high temperatures with this material.

3.3. *Stability studies*

In order to evaluate the catalyst stability, the evolution of the

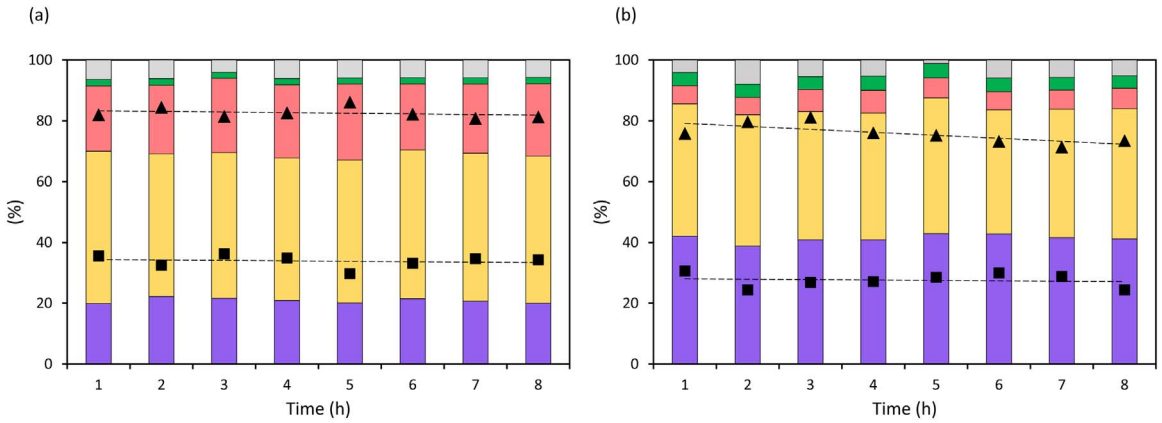

Fig. 7. Stability analyses at 673 K in the gas phase ethanol condensation when is catalyzed by (a) Mg-Al, and (b) Mg-Zr. (WHSV = 7.9 h^{-1}; catalyst mass: 150 mg; 32 vol.% of ethanol). *(See Fig. 2 for codes).*

conversion and selectivity with time on stream was recorded at two different temperatures (673 and 723 K). In order to gain further understanding about the deactivation causes, DRIFT spectra at different exposition times were recorded. Additionally, samples used in the fixed bed reactor were characterized in order to determine the importance of the different deactivation causes: sintering, metal leaching, and fouling by a partial or global blockage of the active sites by permanent adsorption of undesired condensation adducts or butadiene oligomers.

Results obtained at 673 K, both in gas phase (Fig. 7) and also by DRIFT spectroscopy (Fig. 8), suggest that no relevant deactivation was observed at these conditions. Similar conversions, selectivities (higher alcohols selectivities included in Tables S4 and S5) and carbon balances were obtained with the time on stream for both materials, without observing any significant change in the adsorption modes. Among the differences in the DRIFT spectra between both catalysts, the band at 1655 cm^{-1}, related to polybutadiene formation [52], is only slightly observed in the case of Mg-Zr (Fig. 8b), whereas it does not appear with the Mg-Al (Fig. 8a). In addition, the intensity of this band does not increase with reaction time.

Different behavior was observed in gas phase results obtained at 723 K, as it is summarized in Fig. 9. At these conditions, a loss of activity was observed for both materials, being more relevant in the case of Mg-Zr. Thus, conversion decreases from 47.5 to 37.0% with Mg-Al, and from 45.3 to 23.2% with Mg-Zr. Concerning to the carbon balance closure, this parameter increases with the time on stream, reaching final values of 84.2 and 91.4% for Mg-Al and Mg-Zr, respectively, after 8 h. This increase in the carbon balance, mainly in the case of Mg-Zr, is justified by the methodology used to calculate this parameter, taking into account all the compounds of the Scheme 1 (also the reactant). At low conversions, the relative weight of the reactant concentration increase, increasing also the mass balance closure. Main differences between both materials concern to the product selectivities. In the case of Mg-Al, the product distribution is not influenced by the catalyst deactivation, suggesting that the active sites for the main reactions are hardly affected by this deactivation. In good agreement with this hypothesis, differences lower than 2% are observed in selectivities after 1 and 8 h. On the other hand, Mg-Zr results show a relevant decrease in the ethylene selectivity in more than 15%. As a consequence of this deactivation in the side reaction, there is a relative increase of almost 13% in the 1-butanol selectivity, resulting into a constant 1-butanol yield of 3% during all the time tested. Moreover, selectivities to higher alcohols increased with the time on stream (Table S6), whereas they kept constant when Mg-Al was used (Table S7).

The hypothesis of deactivation by crystallographic changes of the active phases was discarded by analyzing the XRD spectra of materials recovered after 8 h on stream at 723 K. The comparison between fresh and spent spectra of both materials is detailed in Fig. 10. No significant changes were observed in any case, with only a slight decrease in the intensity of periclase peaks of Mg-Al. The decomposition of the initial material as well as the deposition of any crystalline phase that can modify the initial activity is then discarded. Possible changes in the surface morphology were also analyzed by N_2 physisorption, obtaining values of 160 and 40 $m^2\ g^{-1}$, for Mg-Al and Mg-Zr, respectively. These values imply a relative decrease twice higher in the case of Mg-Zr (respect to their initial values), suggesting a deactivation by deposition of organic deposits leading to the selective blockage of some active sites. If this deposition is caused by oligomers or large molecules, their adsorption can fully block the pores, justifying the surface area losses.

The assumption of oligomers adsorption was tested by analyzing the evolution of the DRIFT spectra during the same period recorded at similar conditions (Fig. 11). As it could be expected, higher changes are observed in the Mg-Zr spectra, whereas only a slight increase in almost

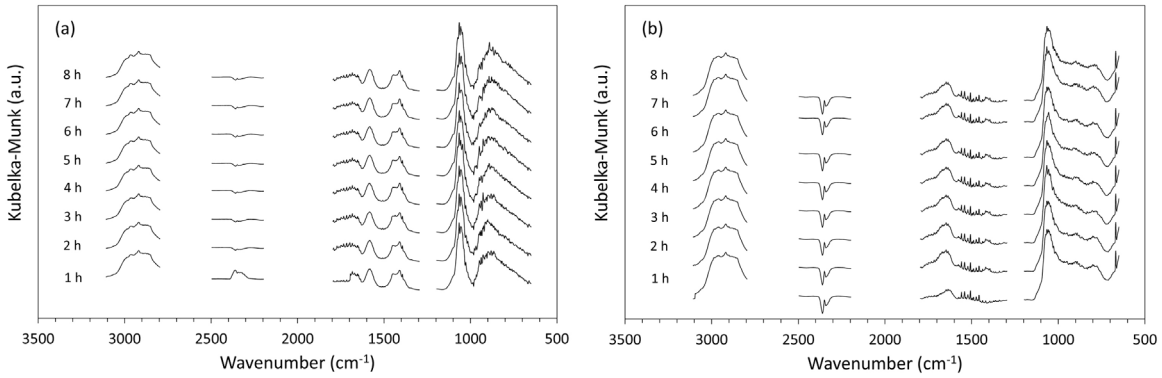

Fig. 8. Evolution of the species adsorbed on the catalytic surface of (a) Mg-Al and (b) Mg-Zr as function of the reaction time when the gas phase ethanol condensation is carried out at 673 K.

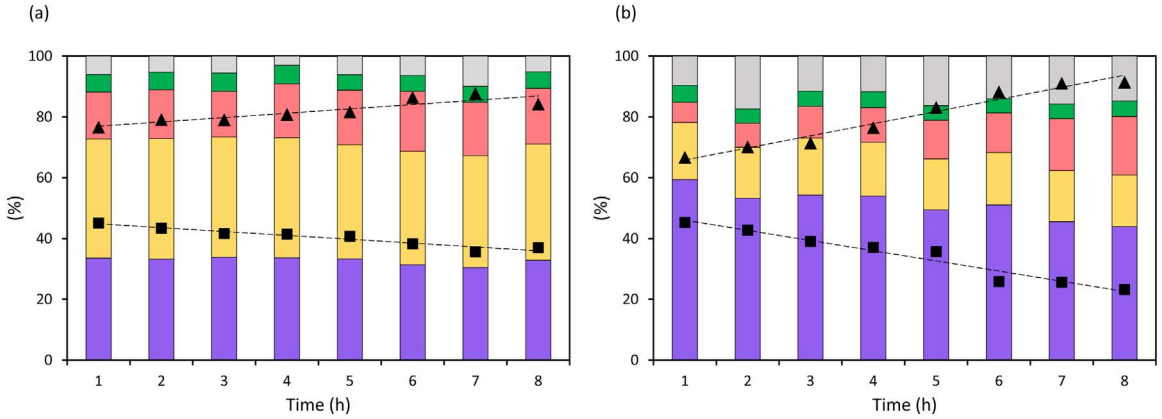

Fig. 9. Stability analyses at 723 K in the gas phase ethanol condensation when is catalyzed by (a) Mg-Al, and (b) Mg-Zr. (WHSV = 7.9 h^{-1}; catalyst mass: 150 mg; 32 vol.% of ethanol). *(See Fig. 2 for codes).*

all the intensities, proportional with the time, is observed with the Mg-Al. In the case of Mg-Zr, there is a relevant increase in the intensities of signals in range 600–1200 cm^{-1} (mainly the band at 750 cm^{-1}) and in 2800–3000 cm^{-1}. According to the previous identification, these rises are directly related to an increase in the amount of alcohols with four or more CH_2 groups (higher alcohols) permanently adsorbed as alkoxides on the acid sites of the catalytic surface, justifying the decrease of the ethylene selectivity during the reaction time as a consequence of the acid sites blockage. This deactivation has been previously reported for different reactions involving the presence of heavy alcohols as reactants, products or intermediates [53,54]. The band associated to polybutadiene (1655 cm^{-1}) was again observed with low intensity with the Mg-Zr material at this temperature. However, the intensity of this band remains almost constant during all the period, suggesting that butadiene oligomerization products play a minor role on catalyst deactivation.

In order to identify the products adsorbed on the catalytic surface, spent samples of both catalysts after 8 h of reaction at 723 K were recovered and analyzed by thermogravimetry in an oxidant atmosphere. Resulting plots are shown in the Supplementary material (Fig. S3). In both cases, main peak appears around 790 K (there are others at lower temperatures related to water and reaction products well identified), suggesting that same or very similar oligomers are deposited on both surfaces. This temperature is considerably higher than the boiling points of the side products detected by GC–MS when the spent materials are extracted with tetrahydrofuran (THF): pentanal with both materials and also 1-nonanol, cresol and 2-ethylphenol with Mg-Zr, suggesting that the oligomerization of oxygenated compounds follows to heavier and THF-insoluble compounds. Comparing both areas, the signal obtained with Mg-Zr corresponds to a 27.4% of the total loss of mass, whereas it means only 11.2% when Mg-Al is used.

These results justify the highest loss of activity observed with the Mg-Zr by the coexistence of two deactivation mechanism: the partial blockage of a greater amount of active sites by the permanent deposition of these oxygen-containing oligomers, generated by successive aldol condensation-dehydration steps, and therefore needing both the presence of acid and basic sites. These oligomers present a strong interaction with acid sites (formation of alkoxides) and also lead to typical fouling effects.

4. Conclusions

The ethanol condensation over mixed oxides for obtaining butanol is studied in this work. The combination of fixed bed reactor experiments, in situ DRIFT measurement and conventional off-site characterization techniques allows to understand the main deactivation causes.

Concerning to the reaction conditions, different temperatures, as well different residence times, were tested, concluding that best results are obtained using 150 mg of catalyst and temperatures from 673 to 723 K: 37.1% of ethanol conversion with 33.4% of 1-butanol selectivity. Similar conversion was obtained with Mg-Zr (30.6%), but this catalyst is less selective to 1-butanol (only 8% at these conditions), increasing the relevance of compounds produced by dehydration steps (ethylene, 1,3-butadiene and diethyl ether). In both cases, carbon balances higher than 70% were obtained at optimum conditions. DRIFT spectroscopy justifies these results by the permanent adsorption of alkoxydes species on the Mg-Zr surface promoted by its higher acidity.

The deactivation of these materials was deeply studied, analyzing the evolution of both, gas phase and catalytic surface, during 8 h at different temperatures. No significant loss of stability with any of these materials was observed at 673 K and lower temperatures. On the other hand, in spite of the catalyst used, a partial deactivation was observed at 723 K, with significant decrease in the ethanol conversion (22.1 and

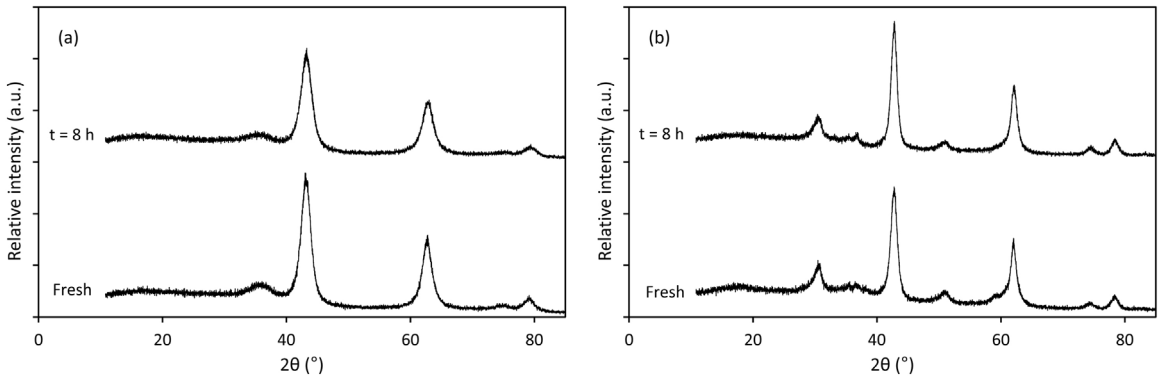

Fig. 10. XRD spectra of fresh and spent materials recovered after 8 hours of ethanol gas phase condensation at 723 K. (a) Mg-Al; (b) Mg-Zr. *(See Fig. 6 for peaks identification).*

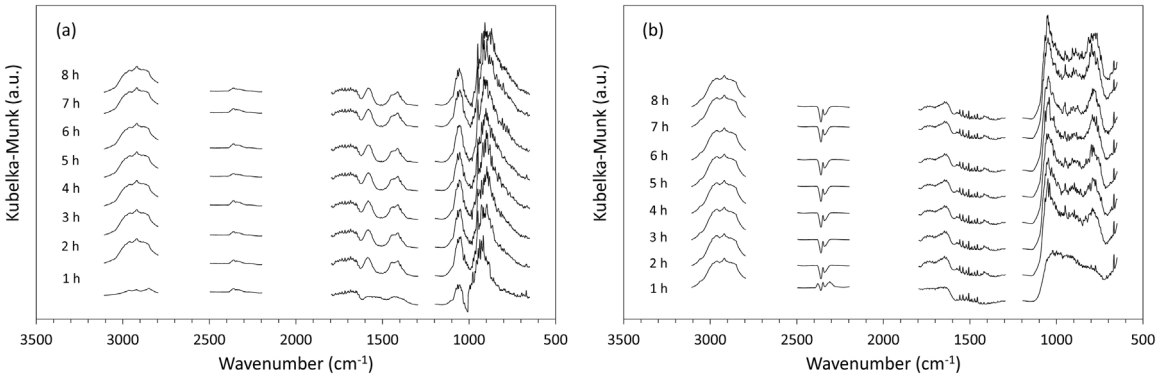

Fig. 11. Evolution of the species adsorbed on the catalytic surface of (a) Mg-Al and (b) Mg-Zr as function of the reaction time when the gas phase ethanol condensation is carried out at 723 K.

13.7% with Mg-Zr and Mg-Al, respectively). DRIFT spectroscopy analyses conclude that this deactivation is due to the permanent adsorption of some intermediates as well as the formation of oxygenated oligomers with more than four carbon atoms, presenting a strong interaction with the catalyst acid sites (surface alkoxides).

Acknowledgments

The authors would like to acknowledge financial support for this work from the Ministry of Economy and Competitiveness of the Spanish Government (Contract CTQ2014-52956-C3-1-R) and from the Government of the Principality of Asturias (Contract FC-15-GRUPIN14-078). Jorge Quesada would also like to thank the Government of the Principality of Asturias for his Ph.D. fellowship of the Severo Ochoa Program (PA-14-PF-BP14-105). Jennifer Cueto is acknowledged by her cooperation in the TG analyses.

Appendix A. Supplementary data

Supplementary data associated with this article can be found, in the online version, at http://dx.doi.org/10.1016/j.apcata.2017.06.001.

References

[1] K. Breitkreuz, A. Menne, A. Kraft, Biofuels Bioprod. Biorefin. 8 (2014) 504–515.
[2] Renewable Fuels Association analysis of public and private estimates, Industry Statistics: 2016 World Fuel Ethanol Production, Renewable Fuels Association Website. http://www.ethanolrfa.org/resources/industry/statistics/#145409899647-8715d404-e546 (Accessed 4 April 2017).
[3] J.T. Kozlowski, R.J. Davis, ACS Catal. 3 (2013) 1588–1600.
[4] E.V. Makshina, M. Dusselier, W. Janssens, J. Degrève, P.A. Jacobs, B.F. Sels, Chem. Soc. Rev. 43 (2014) 7917–7953.
[5] L. Silvester, J.F. Lamonier, J. Faye, M. Capron, R.N. Vannier, C. Lamonier, J.L. Dubois, J.L. Couturier, C. Calais, F. Dumeignil, Catal. Sci. Technol. 5 (2015) 2994–3006.
[6] T.J. Schwartz, B.H. Shanks, J.A. Dumesic, Curr. Opin. Biotechnol. 38 (2016) 54–62.
[7] J. Sun, Y. Wang, ACS Catal. 4 (2014) 1078–1090.
[8] W. Kamiński, E. Tomczak, A. Górak, Ecol. Chem. Eng. S 18 (2011) 31–37.
[9] J.I. Di Cosimo, C.R. Apesteguía, M.J.L. Ginés, E. Iglesia, J. Catal. 190 (2000) 261–275.
[10] M.J.L. Ginés, E. Iglesia, J. Catal. 176 (1998) 155–172.
[11] A.M. Hilmen, M. Xu, M.J.L. Ginés, E. Iglesia, Appl. Catal. A Gen. 169 (1998) 355–372.
[12] E. Billig, A. Seidel, J.I. Kroschwitz (Eds.), Kirk-Othmer Encyclopedia of Chemical Technology, Vol. 4 Wiley-Interscience, New York, 2007p. 398.
[13] O. Fuchs, W. Querfurth, US Patent 1992480 (1935).
[14] E.E. Burgoyne, US Patent 2645667 (1953).
[15] Y. Ono, T. Baba, Catal. Today 38 (1997) 321–337.
[16] K. Tanabe, W.F. Hölderich, Appl. Catal. A Gen. 181 (1999) 399–434.
[17] C. Yang, Z. Meng, J. Catal. 142 (1993) 37–44.
[18] A.S. Ndou, N. Plint, N.J. Coville, Appl. Catal. A Gen. 251 (2003) 337–345.
[19] T. Tsuchida, S. Sakuma, T. Takeguchi, W. Ueda, Ind. Eng. Chem. 45 (2006) 8634–8642.
[20] A. Chieregato, J.V. Ochoa, C. Bandinelli, G. Fornasari, F. Cavani, M. Mella, ChemSusChem 8 (2015) 377–388.
[21] T. Tsuchida, J. Kubo, T. Yoshioka, S. Sakuma, T. Takeguchi, W. Ueda, J. Catal. 259 (2008) 183–189.
[22] S. Ogo, A. Onda, K. Yanagisawa, Appl. Catal. A Gen. 402 (2011) 188–195.
[23] T. Moteki, D.W. Flaherty, ACS Catal. 6 (2016) 4170–4183.
[24] J.I. Di Cosimo, V.K. Díez, M. Xu, E. Iglesia, C.R. Apesteguía, J. Catal. 178 (1998) 499–510.
[25] C.R. Ho, S. Shylesh, A.T. Bell, ACS Catal. 6 (2016) 939–948.
[26] S. Hanspal, Z.D. Young, H. Shou, R.J. Davis, ACS Catal. 5 (2015) 1737–1746.
[27] Z.D. Young, S. Hanspal, R.J. Davis, ACS Catal. 6 (2016) 3193–3202.
[28] M. León, E. Díaz, A. Vega, S. Ordóñez, A. Auroux, Appl. Catal. B Environ. 102 (2011) 590–599.
[29] J.T. Kozlowski, R.J. Davis, J. Energy Chem. 22 (2013) 58–64.
[30] S. Ogo, A. Onda, Y. Iwasa, K. Hara, A. Fukuoka, K. Yanagisawa, J. Catal. 296 (2012) 24–30.
[31] P.E. Hathaway, M.E. Davis, J. Catal. 119 (1989) 497–507.
[32] T.W. Birky, J.T. Kozlowski, R.J. Davis, J. Catal. 298 (2013) 130–137.
[33] C. Angelici, F. Meirer, A.M.J. van der Eerden, H.L. Schaink, A. Goryachev, J.P. Hofmann, E.J.M. Hensen, B.M. Weckhuysen, P.C.A. Bruijnincx, ACS Catal. 5 (2015) 6005–6015.
[34] I.C. Marcu, N. Tanchoux, F. Fajula, D. Tichit, Catal. Lett. 143 (2013) 23–30.
[35] L.E. Iton, I. Choi, J.A. Desjardins, V.A. Maroni, Zeolites 9 (1989) 535–538.
[36] C.S. Polster, H. Nair, C.D. Baertsch, J. Catal. 266 (2009) 308–319.
[37] E. Río, S.E. Collins, A. Aguirre, X. Chen, J.J. Delgado, J.J. Calvino, S. Bernal, J. Catal. 316 (2014) 210–218.
[38] J. Quesada, L. Faba, E. Díaz, S. Bennici, A. Auroux, S. Ordóñez, J. Catal. 329 (2015) 1–9.
[39] J.T. Kozlowski, M. Behrens, R. Schlögl, R.J. Davis, ChemCatChem 5 (2013) 1989–1997.
[40] L. Faba, E. Díaz, S. Ordóñez, Appl. Catal. B Environ. 142–143 (2013) 387–395.
[41] M.E. Davis, R.J. Davis, Fundamentals of Chemical Reaction Engineering, in: E.A. Jones (Ed.), McGraw Hill, New York, 2003, pp. 190–205.
[42] M. Dömök, M. Tóth, J. Raskó, A. Erdőhelyi, Appl. Catal. B Environ. 69 (2007) 262–272.
[43] T.L. Jordison, L. Peereboom, D.J. Miller, Ind. Eng. Chem. Res. 55 (2016) 6579–6585.
[44] J.E. Rekoske, M.A. Barteau, Ind. Eng. Chem. Res. 50 (2011) 41–51.
[45] S. Shylesh, A.A. Gokhale, C.D. Scown, D. Kim, C.R. Ho, A.T. Bell, ChemSusChem 9 (2016) 1462–1472.
[46] J.E. Rekoske, M.A. Barteau, Langmuir 15 (1999) 2061–2070.
[47] T. Shimanouchi, U.S. National Bureau of Standards (Ed.), Tables of Molecular Vibrational Frequencies Consolidated, Vol. I U.S. Government Printing Office, Washington, 1972, pp. 1–160.
[48] B.C. Smith, Infrared Spectral Interpretation: A Systematic Approach, CRC Press LLC, Florida, 1999 p. 36.
[49] I. Sádaba, M. Ojeda, R. Mariscal, J.L.G. Fierro, M. López-Granados, Appl. Catal. B Environ. 101 (2011) 638–648.
[50] C.J. Barrett, J.N. Chheda, G.W. Huber, J.A. Dumesic, Appl. Catal. B Environ. 66 (2006) 111–118.
[51] S. Ordóñez, E. Díaz, M. León, L. Faba, Catal. Today 167 (2011) 71–76.
[52] H. Berndt, H. Landmesser, J. Mol. Catal. A Chem. 197 (2003) 245–253.
[53] A. de Klerk, E. Furimsky, Catalysis in the Refining of Fischer-Tropsch Syncrude, in: J.J. Spivey (Ed.), RSC Publishing, Cambridge, 2010RSC Catalysis Series No. 4, p. 136.
[54] D. Leckel, Energy Fuel 21 (2007) 662–667.